Opto-Electronics Review

journal homepage: https://journals.pan.pl/opelre

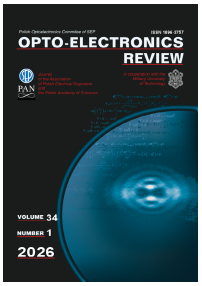

SCL-band optimised femtosecond high-order fibre Bragg grating for simultaneous strain and temperature measurement

Tomasz Osuch[1,2*], Lena Potkańska[2], Alicja Anuszkiewicz[2], Mariusz Zdanowicz[1]

[1] National Institute of Telecommunications, ul. Szachowa 1, 04-894 Warsaw, Poland
[2] Institute of Electronic Systems, Faculty of Electronics and Information Technology, Warsaw University of Technology, ul. Nowowiejska 15/19, 00-665 Warsaw, Poland

Article info

Article history:
Received 08 Oct. 2025
Received in revised form 03 Feb. 2026
Accepted 16 Feb. 2026
Available on-line 12 Mar. 2026

Keywords:
high-order fibre Bragg gratings;
femtosecond laser manufacturing;
fibre optic sensor;
strain and temperature measurement

Abstract

Design and femtosecond laser fabrication of high-order fibre Bragg gratings with precisely controlled absolute wavelengths and spectral separation between higher-order resonances are presented. The line-by-line inscription technique ensures relatively high and similar reflection coefficients for neighbouring harmonics. A high-order fibre Bragg grating was fabricated to operate within the SCL-band, matching the spectral range of commercially available fibre optic interrogators. The gratings were experimentally verified as an easy-to-use sensor for accurate simultaneous strain and temperature discrimination. The proposed approach addresses key limitations in dual-parameter sensing through a single compact structure, flexible spectral design, and straightforward application and compatibility with existing interrogation systems.

1. Introduction

Fibre Bragg gratings (FBGs) are widely recognised in metrology as sensors for various physical parameters. Their main advantages are high accuracy and sensitivity, as well as wavelength multiplexing capability. These enable the use of FBGs in quasi-distributed sensing systems and the simultaneous measurement of multiple parameters. Bragg gratings written in commonly used silica optical fibres are resistant to strong magnetic fields and can operate in harsh environmental conditions. Moreover, their small size, low weight, multiple encapsulation possibilities increase their application potential in various industries, such as energy production and storage [1, 2], oil and gas industry [3, 4], transport [5, 6], civil engineering [7–9], medicine [10, 11] or biosensing [12].

Among many others, the most common application of the FBG is structural health monitoring (SHM). These include measuring physical quantities such as temperature, strain, inclination, pressure, and transverse force. However, the crucial disadvantage of mechanical parameter measurement using a single FBG is temperature cross-sensitivity. In practical applications, this means it is impossible to achieve correct strain demodulation from the Bragg wavelength shift when temperature changes. In other words, simultaneous measurement of the strain and temperature with a single FBG is problematic.

Over the years, the cross-sensitivity problem of FBG has been addressed with various methods. One of the proposed solutions was a hybrid sensing structure comprising a standard FBG combined with a long-period grating [13] or an FBG with a Fabry-Pérot (FP) resonator [14]. Another approach uses an FBG in a tapered optical fibre, which provides distinct temperature (only wavelength shift) and strain (wavelength shift and change in spectral width) responses [15]. The main disadvantages of the aforementioned methods are technological complexity and limited multiplexing capability, due to their complex, relatively wide spectra. Moreover, the tapered optical fibre becomes more fragile. Similar problems are present in other devices allowing for simultaneous strain and temperature discrimination, e.g., when splicing two FBGs written in different optical fibres having different outer diameter [16], core diameter [17], core doping concentrations of GeO_2 [18] or inscribed in optical fibres with different dopants [19]. Splicing optical fibres significantly weakens their mechanical properties, limiting

*Corresponding author at: tomasz.osuch@pw.edu.pl

https://doi.org/10.24425/opelre.2026.158113
1896-3757/ Association of Polish Electrical Engineers (SEP) and Polish Academic of Sciences (PAS). Published by PAS

the strain measurement range. Moreover, spliced optical fibres with different core diameters (i.e., different numerical aperture) introduce additional transmission losses and increase the back-reflection level. Similar drawbacks are present in FBG-based sensors with partially reduced diameter by etching [20]. In many applications, the key parameter of the FBG sensor is its compact size. The majority of the structures described above do not meet this requirement.

The cross-sensitivity problem in a single FBG-based sensor has also been intensively studied over the years. The device proposed by Chen *et al*. used a high-birefringent (Hi-Bi) side-hole optical fibre for simultaneous temperature and strain measurements [21]. In this approach, a Hi-Bi optical fibre ensures clear separation between the polarisation-dependent Bragg resonances, which is challenging to achieve, particularly with commercially available Hi-Bi fibres and in applications requiring relatively short gratings, which inherently result in a wider spectrum. To resolve overlapping peaks in such cases, advanced spectrum reconstruction methods are essential [22]. Air-filled side holes result in different temperature sensitivities between the fast and slow axes due to their different thermo-optic coefficients. However, such a device requires additional polarisation control to excite two polarisation modes. Moreover, a Hi-Bi optical fibre is not compatible with commercial polarisation-insensitive interrogators used with standard single-mode optical fibres (SMFs).

A single FBG can be discriminated between temperature and strain by exploiting the core-cladding mode coupling of a tilted fibre Bragg grating (TFBG). The spectrum of such a TFBG comprises Bragg peaks corresponding to the core and cladding modes, which exhibit different thermal sensitivities, whereas the strain sensitivities are approximately equal [23]. However, the usefulness of TFBGs in combination with interrogators is severely limited by their complex spectra, particularly due to the numerous cladding peaks observed in transmission. It has also been demonstrated that obtaining reliable and unambiguous temperature and strain measurements requires advanced spectral analysis methods [24].

Bardy *et al*. proposed a single FBG with saturation in index perturbation. In such a grating, both fundamental Bragg reflection ($\lambda_B = 1561$ nm) and second-harmonic peak ($\lambda_{2B} = 789$ nm) are observed in the measured spectra [25]. The main disadvantage of the proposed grating is that the reflection efficiency at the second-harmonic Bragg wavelength is as low as 0.1% and the optical fibre is no longer single-mode in this spectral range. These features, together with a very large separation between the wavelength peaks (c.a. 770 nm), require a complex and expensive measurement system, which makes it impractical for real-world applications. The latter drawback is also evident in the two-superimposed-FBGs approach [26]. An alternative method for a single-FBG fabrication with harmonic reflections is to use a phase mask optimised for IR radiation and a femtosecond laser [27, 28]. In this case, the two series of Bragg minima are observed in the measured spectrum. The first resonance minima correspond to half of the phase mask period and are the result of the interference of +1st and −1st diffraction orders. The secondary set of spectra corresponds to the full phase-mask period due to the interference between the 1st and 0th diffraction orders. It was shown that each resonance peak has different temperature and strain coefficients. Although harmonic reflections are observed in the grating spectral response, the wavelength spacing between adjacent minima falls outside the spectral range of the SCL-band-optimised interrogators available on the market. Large discrepancies in the reflection coefficients of harmonics (up to 20–30 dB) are also unfavourable. Using phase masks with a larger pitch to obtain a shorter harmonic wavelength spacing increases the number of diffraction orders, thereby reducing the fringe visibility of the interfered diffracted beams. It finally deteriorates the quality and repeatability of the gratings formation. These drawbacks, together with the inherent lack of flexibility of the phase mask method, significantly limit its widespread use.

In this paper, we present a method for designing and fabricating a high-order fibre Bragg grating (HO-FBG) with a flexibly tailored wavelength spacing between adjacent harmonic reflections. The proposed HO-FBG can be used for efficient and easy-to-use simultaneous strain and temperature discrimination. The advantage of the proposed design method is the ability to adjust the HO-FBG parameters to fit within the spectral range of commercially available interrogators, which typically operate in the S (1460–1530 nm), C (1530–1565 nm), and L (1565–1625 nm) bands.

The method for HO-FBG design is described in section 2. The fabrication process and spectral characterisation of HO-FBG are presented in section 3. Due to the fact that temperature and strain sensitivities are different between the m-th and $(m+1)$-th reflection orders, the possibility of simultaneous strain and temperature measurement and error analysis are presented in section 4. The last section 5 summarises the work.

2. HO-FBG design

Let us assume that the optical fibre interrogator operates in the spectral range $\langle\lambda_L; \lambda_H\rangle$. Moreover, let us assume that the maximum Bragg wavelength shift of the HO-FBG due to strain and/or temperature changes is equal to $\Delta\lambda_{margin}$. Therefore, taking into account this margin, the Bragg wavelengths of two adjacent HO-FBG orders should lie within the spectral range $\langle\lambda_{MIN}; \lambda_{MAX}\rangle$, where $\lambda_{MIN} = \lambda_L + \Delta\lambda_{margin}$ to $\lambda_{MAX} = \lambda_H - \Delta\lambda_{margin}$. Considering the HO-FBG equation:

$$m \cdot \lambda_{B,m} = 2 \cdot n_{\text{eff}} \cdot \Lambda\,, \tag{1}$$

where m is the resonance order, $\lambda_{B,m}$ stands for the Bragg wavelength of the m-th resonance, n_{eff} denotes the effective refractive index of the fibre core, and Λ stands for the grating period. Relations for m-th and $(m+1)$-th order Bragg wavelengths should fulfil the following equations:

$$\lambda_{B,m+1} \geq \lambda_{MIN} = 2 \cdot n_{\text{eff}} \cdot \Lambda / (m+1), \tag{2}$$

$$\lambda_{B,m} \leq \lambda_{MAX} = 2 \cdot n_{\text{eff}} \cdot \Lambda / m. \tag{3}$$

Simple transformation of (2) and (3) allows for the estimation of m, at which the m-th and $(m+1)$-th order

HO-FBG resonant wavelengths are located within the desired spectral range $<\lambda_{MIN}; \lambda_{MAX}>$:

$$m = \lambda_{MIN} / \left(\lambda_{MAX} - \lambda_{MIN}\right), \quad (4)$$

where the constant n_{eff} value is assumed within the above spectral range. The above relation, combined with (2) or (3), can be used for evaluating the grating period Λ. The minimal m-value that fulfils the design assumption regarding the spectral positions of the m-th and $(m+1)$-th HO-FBG reflection peaks also ensures the minimum achievable grating period and thus the grating length. In turn, the minimisation of grating length provides a uniform temperature and strain distribution along its length, which plays a crucial role in accurate sensing.

In this work, a HYPERION SI255 interrogator from Luna, with the spectral range from 1460 nm to 1620 nm, was used. We also assumed that the maximum Bragg wavelength shift due to strain/temperature changes is $\Delta\lambda_{margin} = 10$ nm. This in turn gives $\lambda_{MIN} = 1470$ nm, $\lambda_{MAX} = 1610$ nm. Then, using (4), it is straightforward to calculate that $m = 10.5$. Due to the fact that m is an integer, it is taken to be $m = 11$. This means that in the assumed spectral range of the interrogator, $m = 11$ and $m = 12$ orders of the Bragg resonance are observed. Since the calculated value of m has been rounded up, the grating periods calculated after transforming (2) and (3) for $n_{eff} = 1.45$ are $\Lambda_{m+1} = 6.083$ μm and $\Lambda_m = 6.107$ μm, respectively. Taking into account (2), for $\lambda_{B,m+1} \geq \lambda_{MIN}$, the period must satisfy the following condition $\Lambda \geq \Lambda_{m+1}$. Similarly, from (3) it follows that for $\lambda_{B,m} \leq \lambda_{MIN}$,, it must be ensured that $\Lambda \leq \Lambda_{m+1}$. Since, for m = 11, $m > m+1$, the resultant grating period can be calculated as the average of Λ_{m+1} and Λ_m, i.e., $\Lambda = 6.094$ μm. Then, the expected Bragg wavelengths of m-th and $(m+1)$-th orders are $\lambda_{B,m+1} = 1472.7$ nm and $\lambda_{B,m} = 1606.6$ nm, respectively and fall within the assumed range ⟨1470 nm;1610 nm⟩.

The choice of the minimum integer $m = 11$ that satisfies the design criteria is fundamental for ensuring optimal sensing performance. By selecting the lowest possible order, we maximise the spectral separation between adjacent harmonics ($\Delta\lambda \approx 134$ nm) within the 160 nm interrogation window of the HYPERION SI255. This maximal separation is crucial for dual-parameter sensing, as it exploits the wavelength-dependent nature of the thermo-optic and stress-optic coefficients over the broadest possible range, thereby enhancing the diversity of the sensitivity matrix coefficients. Furthermore, this design leaves a strategic 10 nm buffer at each edge of the interrogator range, ensuring that both resonance peaks remain detectable even under high strain or temperature changes without reaching the device spectral boundaries.

3. HO-FBG fabrication and spectral characterisation

A designed fibre Bragg grating was inscribed in the micro-machining workstation equipped with an NKT Origami XP femtosecond laser operating at 1031 nm with a pulse duration of 320 fs. The pulse energy was controlled with an acousto-optic modulator (AOM) and a beam splitter to be approximately 0.5 μJ in the fibre core. The laser beam was focused by the microscope objective with a numerical aperture $NA = 0.75$.

The Bragg grating was inscribed with a line-by-line method over the section of the SMF (SMF-28, Corning, USA). The optical fibre was mounted on a high-precision air-bearing translation stage, moving at a constant velocity of 8 μm/s relative to the laser focal point. The femtosecond laser operated at a repetition rate of 50 kHz. Each of the 1001 grating planes was formed by a transverse scan of the laser beam, lasting approximately 1 s per line, ensuring that each line is composed of multiple overlapping pulses to induce a stable, uniform refractive index change across the entire core diameter. To achieve the periodic structure, an AOM was employed as a high-speed optical shutter synchronised with the translation stage. The grating was fabricated using a raster-scan trajectory to ensure high structural uniformity: each transverse line was inscribed across the core in the same direction at a velocity of 8 μm/s. Upon completion of a line, the AOM blocked the beam while the stage performed a 2D repositioning move, returning to the initial transverse starting side and advancing by the grating pitch ($\Lambda = 6.09$ μm) to begin the next period. This process was repeated for 1001 lines, resulting in a total grating length of 6.09 mm.

Additionally, the effectiveness of the femtosecond laser beam focusing on the fibre core and the precise location of the fabricated structure were on-line monitored using an optical backscatter reflectometer OBR 4600 Luna integrated with a laser micromachining workstation. The area of the processed optical fibre was monitored in real time by transmission light microscopy throughout the grating fabrication process. The microscope image of the fragment of in-written HO-FBG is presented in Fig. 1.

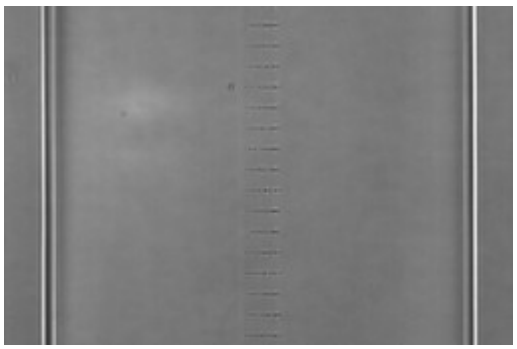

Fig. 1. Microscope image of the fabricated HO-FBG.

After the HO-FBG fabrication, it was spectrally characterised by a Yokogawa AQ6370D optical spectrum analyser with a 0.05 nm wavelength resolution. The optical fibre with HO-FBG was excited by the broadband source with a central wavelength of 1550 nm. The measured spectra of the fabricated HO-FBG in the ambient environment (temperature $T_0 = 25$ °C, no strain applied $\varepsilon = 0$ με) are presented in Fig. 2.

The resonance wavelengths are $\lambda_{B,m=12} = 1470.0$ nm and $\lambda_{B,m=11} = 1601.6$ nm, respectively. These values are consistent with the calculation. Small discrepancies are due to rounding of calculation results during design, limited precision in refractive index of the fibre core estimation (c.a. 0.003), limited resolution of the period setting in micromachining workstation software resulting from the minimum incremental motion (MIM) of the translation stages (2 nm), chromatic dispersion of the optical fibre

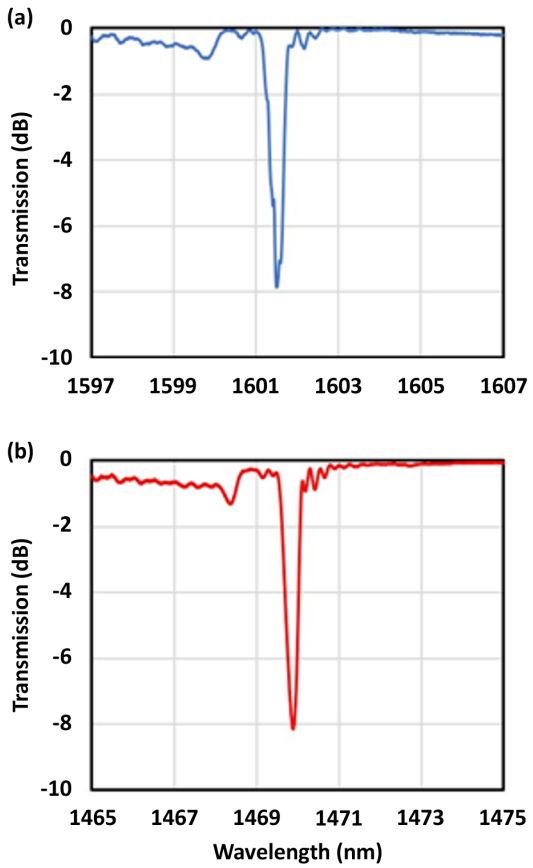

Fig. 2. Transmission spectra of the fabricated HO-FBG for (a) m =11 order, (b) m =12 order.

introducing small effective refractive index differences across the measured spectrum (c.a. 0.002), and a limited precision in optical fibre positioning (1 μm) and tensioning (up to 100 με) during the grating fabrication process. Among these sources, the MIM and refractive index uncertainty are the most significant, each capable of introducing wavelength discrepancies exceeding 1 nm. It is important to note that these discrepancies result from a combination of deterministic and random factors. However, the absolute initial Bragg wavelength does not degrade sensing performance, as each HO-FBG sensor undergoes rigorous calibration prior to deployment.

The minima of the transmission peaks are $T_{\min,m=12} = -8.1$ dB and $T_{\min,m=11} = -7.9$ dB, which translates into reflection coefficients of 85% and 84%, respectively. Full width at half maximum (FWHM) for both resonance peaks is the same and equals 0.38 nm.

The line-by-line technique of gratings inscription exhibits a great flexibility in tailoring both absolute harmonic wavelengths and their spectral separation. Using ultra-precision translation stages in a micromachining workstation, the grating period can be adjusted with nanometre steps, yielding sub-nanometre resolution in both resonant wavelengths and spectral distances of Bragg-wavelength high-order harmonics.

The spectral response of the fabricated HO-FBG is governed by the general Bragg condition described by (1). In conventional gratings fabricated using a phase mask, a sinusoidal refractive index modulation is typically obtained that excites the first-order resonance ($m = 1$). In practice, higher-order reflections ($m > 1$) can appear due to the presence of non-ideal interference patterns (e.g., from the 0th or higher-diffraction orders of the phase mask) or due to the refractive index saturation in highly photosensitive optical fibres. Such saturation effectively ”lips” the peaks of the sinusoidal index modulation, leading to a profile that resembles a rectangular profile, which inherently generates higher-order harmonics. However, distorting the sinusoidal refractive index profile to achieve higher-order reflections in the phase-mask technique is a poorly controlled process – often occurring as a side effect – and these higher orders remain weak, decaying rapidly as the reflection order m increases.

In contrast, the line-by-line femtosecond laser inscription intentionally employs a non-sinusoidal, step-like refractive-index modification. Since each inscribed line is significantly narrower than the grating period (as it is shown in Fig. 1), the structure exhibits a very low duty cycle. From a Fourier analysis perspective, this narrow spatial modulation is exceptionally rich in higher-order spatial harmonics. Unlike the unintentional harmonics in phase-mask-based gratings caused by refractive index saturation or a non-ideal interference pattern generated just behind the phase mask, the HO-FBG harmonics are a direct result of the high-contrast, well-localised structural modifications.

The efficiency of these high-order resonances is also highly dependent on the peak intensity of the laser pulses used during inscription. The laser energy must be carefully optimised to exceed the nonlinear absorption threshold of the silica glass, thereby creating a permanent, high-contrast change in the refractive index. If the pulse energy is too low, the induced index modulation is insufficient to produce a detectable Bragg peak at high orders. Conversely, excessive energy can cause glass damage, increasing scattering losses and degrading spectral quality. In this work, the laser intensity was precisely maintained to produce sharp, high-contrast lines.

4. HO-FBG sensing characterisation

In the next step, the HO-FBG was characterised using a fibre optic interrogator, Luna HYPERION SI255, to determine its sensitivity to temperature and strain. The reflection spectrum recorded by the interrogator at room temperature when no strain is applied is shown in Fig. 3. It can be seen that the spectral distance between the 11th and 12th order reflection peaks and the edges of the measurement window of the interrogator is approximately 10 nm, which is in accordance with the design assumption.

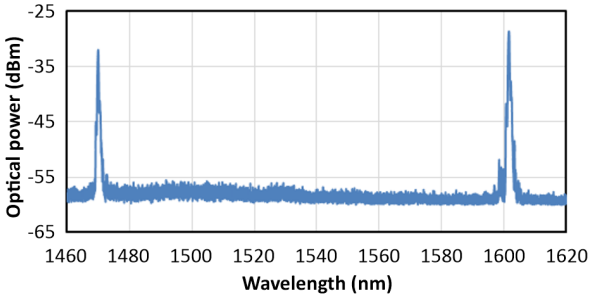

Fig. 3. Reflected spectrum of the HO-FBG measured by means of fibre optic interrogator.

First, the temperature response of the HO-FBG was examined. The HO-FBG was placed on the Ohaus Guardian 500 hotplate with adjusted temperature. To improve the accuracy of the temperature reading, the HO-FBG was isolated from the environment and its temperature was controlled using a K-type thermocouple. The temperature was changed from 25 °C to 130 °C in 15 °C steps. For each temperature setting, the reflection spectrum was measured and Bragg wavelengths of both peaks were estimated. The measurements were made at increasing temperature (heating) and then repeated for the same steps at decreasing temperature (cooling). The measurement results of the Bragg wavelengths of the orders $m = 11$ and $m = 12$ *vs*. temperature are presented in Fig. 4.

It can be observed that the characteristics of resonance wavelengths *vs*. temperature changes for both resonant peaks (as well as for heating and cooling) are linear. Therefore, it is possible to approximate the results with a linear function and to determine the slope coefficients, which are temperature sensitivities. The value of the temperature sensitivity coefficient for the $m = 12$ order of the Bragg grating is almost the same as the average value of $K_{T,m=12} = 11.6$ pm/°C. For the resonance peak of the $m = 11$ order, the temperature sensitivity for heating and cooling is $K_{T,m=11} = 12.1$ pm/°C.

The sensitivity to strain was examined by observation of the Bragg wavelength shift when the longitudinal strain is applied to the HO-FBG. The 246 mm section of optical fibre with in-written HO-FBG was elongated from 0 μm to 550 μm in 50 μm increments. It corresponds to the applied strain from 0 to 2236, with 203 steps. Strain measurements were also carried out in two directions: applying the strain from 0 με to 2236 με (stretching) and decreasing the strain from 2236 με to 0 με (releasing). The strain responses of the HO-FBG for orders $m = 11$ and $m = 12$ are presented in Fig. 5. The measurement results reveal that the strain response of HO-FBG is linear over the entire examined range for both resonance orders and both stretching and releasing. The particular series of measurements was approximated with the linear functions and the sensitivities were derived. Estimated strain sensitivities for $m = 12$ and $m = 11$ resonance peaks are $K_{\varepsilon,m=12} = 1.08$ pm/με, and $K_{\varepsilon,m=11} = 1.19$ pm/με, respectively.

Since determined strain and temperature coefficients are different for reflection orders ($m = 11$ and $m = 12$), a matrix equation with non-zero determinant can be constructed as follows:

$$\begin{bmatrix} \Delta\lambda_{B,m=11} \\ \Delta\lambda_{B,m=12} \end{bmatrix} = \begin{bmatrix} K_{\varepsilon,m=11} & K_{T,m=11} \\ K_{\varepsilon,m=12} & K_{T,m=12} \end{bmatrix} \cdot \begin{bmatrix} \Delta\varepsilon \\ \Delta T \end{bmatrix} = \begin{bmatrix} 1.19 & 12.1 \\ 1.08 & 11.6 \end{bmatrix} \cdot \begin{bmatrix} \Delta\varepsilon \\ \Delta T \end{bmatrix}, \tag{5}$$

where $\Delta\lambda_{B,m=12}$ and $\Delta\lambda_{B,m=11}$ are the Bragg wavelength shifts of resonant peaks when strain and/or temperature change is applied. Simple transformation of the above matrix equation gives a direct matrix formula allowing for the explicit determination of temperature ΔT and strain $\Delta\varepsilon$

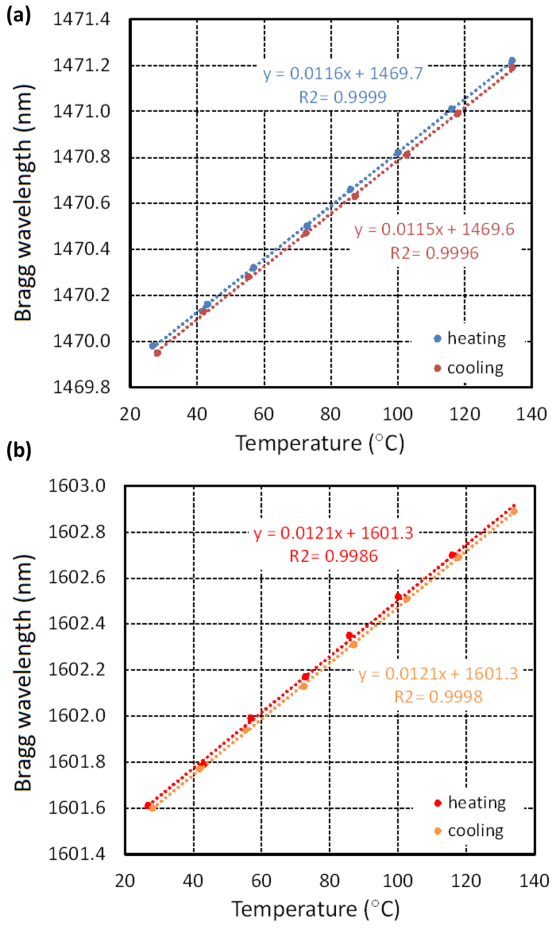

Fig. 4. Results of the temperature characterisation of the HO-FBG for (a) $m = 2$ and (b) $m = 11$ orders.

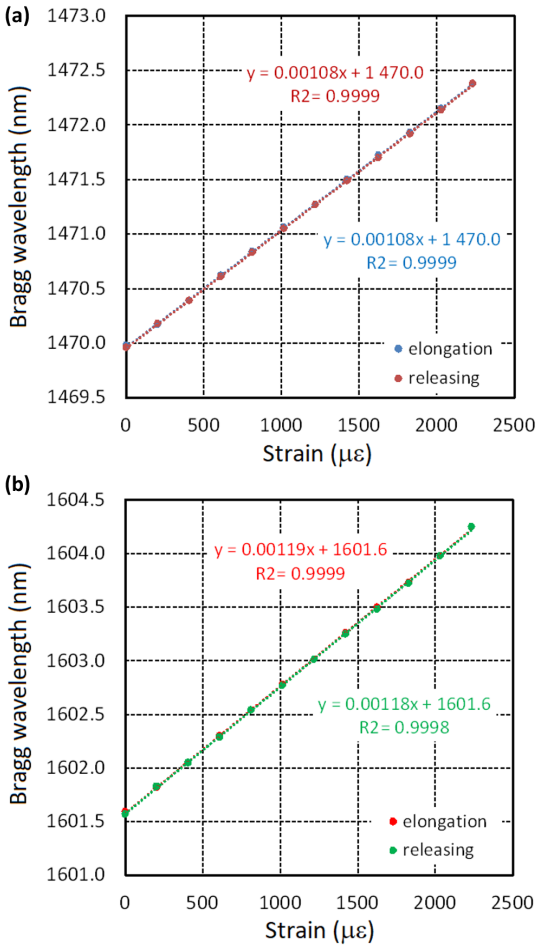

Fig. 5. Results of the strain characterisation of the HO-FBG for (a) $m = 12$ and (b) $m = 11$ orders.

changes basing on measured wavelength shifts $\Delta\lambda_{B,m=12}$ and $\Delta\lambda_{B,m=11}$:

$$\begin{bmatrix}\Delta\varepsilon\\ \Delta T\end{bmatrix}=\frac{1}{D}\cdot\begin{bmatrix}K_{T,m=12} & -K_{T,m=11}\\ -K_{\varepsilon,m=12} & K_{\varepsilon,m=11}\end{bmatrix}\cdot\begin{bmatrix}\Delta\lambda_{B,m=11}\\ \Delta\lambda_{B,m=12}\end{bmatrix}$$
$$=\frac{1}{0.736}\cdot\begin{bmatrix}11.6 & -12.1\\ -1.08 & 1.19\end{bmatrix}\cdot\begin{bmatrix}\Delta\lambda_{B,m=11}\\ \Delta\lambda_{B,m=12}\end{bmatrix}, \quad (6)$$

where $D=K_{\varepsilon,m=11}K_{T,m=12}-K_{T,m=11}K_{\varepsilon,m=12}$. It can be inferred that differences in strain and temperature sensitivities of particular HO-FBG Bragg orders are due to the fact that stress-optic and thermo-optic coefficients of optical fibre glass are wavelength-dependent.

Limited accuracy of the wavelength measurement has a major impact on errors in simultaneous strain and temperature discrimination. To estimate sensing accuracy, an error-ellipse approach can be used [25]. This involves mapping of errors from wavelength space to strain–temperature space. Bragg wavelengths of 11th and 12th harmonics were measured by the fibre optic interrogator with a ± 1 pm wavelength accuracy. Taking into account derived strain and temperature coefficients of particular harmonics and using formulas adopted from [25], the resulting maximum strain and temperature measurement errors are $\Delta_{\text{error}}\varepsilon_{\max}=22.8$ με and $\Delta_{\text{error}}T_{\max}=2.2$ °C, respectively. The errors of the simultaneous strain and temperature discrimination were visually evaluated using the error ellipse approach (Fig. 6). The tilt of the ellipse originates from the inherent correlation between the sensitivity coefficients of the 11th and 12th orders, as both resonances respond to the same physical phenomena. However, the distinct sensitivities of these high-order harmonics prevent the ellipse from collapsing into a line, ensuring a well-conditioned system for parameter decoupling. The narrowness (eccentricity) of the ellipse illustrates the mapping of the ± 1 pm interrogator resolution into the physical domain, yielding a precision of 22.8 με and 2.2 °C. This analysis confirms the practical utility of the sensor: the errors are significantly smaller than the typical measurement ranges in structural health monitoring, while the optimised spectral separation in the SCL-band ensures robust peak tracking. An alternative error analysis presented in [29] assumes the worst-case scenario (in which all errors accumulate), which may overestimate the total error.

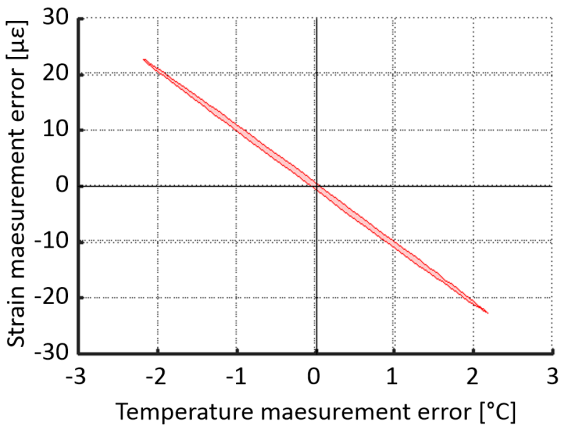

Fig. 6. Error ellipse for HO-FBG.

A comparison of the key metrological properties of several fibre optic structures is presented in Table 1.

Table 1.
Comparison of several strain/temperature sensing methods.

Method [Ref.]	K_T (pm/°C)	K_ε (pm/με)	$\Delta_{\text{err}}\varepsilon$ (με) $\Delta_{\text{err}}T$ (°C)	Meas. range
Hybrid FBG+F-P [14]	13.97 0.82	1.063 1.23	19.6 4.7	0–2500 με 19–600 °C
FBGs in tapered fibre [15]	10.16 9.94	1.01 1.19	9.27 2.08	0–1500 με 20–80 °C
FBGs in spliced fibres (different dopants) [19]	8,43 7.37	0.969 0.949	18.4 2.2	0–1000 με 30–130 °C
FBGs in spliced fibres (different ext. diameters) [16]	7 5.7	0.42 0.949	17 1	0–2500 με 30–150 °C
FBGs in spliced fibres (different core diameters) [17]	12.3 13.2	0.69 0.76	26.7 1.6	0–2000 με 30–90 °C
FBG in Hi-Bi fibre [21]	9.29 8.79	1.31 1.31	19.5 2.8	0–1300 με −50–80 °C
HO-FBG (this work)	11.6 12.1	1.08 1.19	22.8 2.2	0–2236 με 25–130 °C

As demonstrated, the fundamental parameters of the HO-FBG are consistent with other solutions. Notably, it maintains a highly favourable ratio between measurement accuracy and the measurement range. Furthermore, our solution offers unique advantages, including compactness (single, few mm-long in-fibre structure), high spectral adaptability (flexible design enabled by maskless fabrication), low fabrication cost (SMF-based structure), and applicability (interrogator-compatible). The femtosecond (fs) laser inscription technique offers significant cost-efficiency advantages over traditional ultraviolet (UV) laser-based methods. First, femtosecond-laser processing enables direct inscription in standard, non-photosensitive fibres (e.g., SMF-28) without the need for expensive photosensitive fibres or time-consuming pre-treatment processes like hydrogen loading. Second, the flexibility of the line-by-line inscription method allows for the fabrication of gratings with various spectral characteristics through simple software adjustments, bypassing the need for a dedicated, costly phase mask for each specific wavelength. Furthermore, the HO-FBG serves as a dual-parameter sensor integrated into a single structure during a one-step process. This eliminates the technological complexity and labour costs associated with a multi-step fabrication required for hybrid structures, such as two spliced gratings written in separate technological steps in different fibres [16–19], hybrid structures FBG+LPG [13], FBG+FP [14], or FBG written in a previously tapered fibre [15]. Finally, the compatibility of the resulting structure with standard industrial interrogators ensures a lower total cost of ownership for the complete sensing system compared to setups requiring high-resolution optical spectrum analysers.

5. Conclusions

Design and femtosecond-laser fabrication of the HO-FBG that spectrally matches the commercially available optical fibre interrogators operating in SCL-band is presented. Both absolute wavelengths and spectral separation of high-order resonances can be flexibly and precisely tailored. The proposed design approach assumes the use of the full available spectral range of the interrogator, which, on one hand, promotes the separation of resonance peaks and, on the other hand, provides better measurement capabilities, as the sensitivity differences between individual peaks increase with the wavelength difference between them.

Due to the line-by-line fabrication technique, the induced refractive-index changes profile of the HO-FBG supports the formation of higher-order resonances with relatively high reflectance. To prove it, HO-FBG with almost equally reflection efficiencies at 11th and 12th order resonant peaks (at wavelengths of 1601.6 nm and 1470.0 nm, respectively) that perfectly match the assumed spectral range of the HYPERION SI255 interrogator, was designed and fabricated. This HO-FBG was experimentally verified as an easy-to-use sensor for simultaneous strain and temperature discrimination. Due to the optimised spectral separation of adjacent Bragg harmonics, the differences in strain (1.08 pm/με and 1.19 pm/με) and temperature responses (11.6 pm/°C and 12.1 pm/°C) of $m = 12$ and $m = 11$ resonant peaks were obtained. This makes the single HO-FBG suitable for simultaneous strain and temperature discrimination with relatively low maximum measurement errors. The proposed HO-FBG approach offers several distinct advantages over previously reported dual-parameter sensing techniques.

First, unlike cascaded hybrid structures, HO-FBG provides single-point sensing, which ensures a highly compact sensor footprint. By measuring both parameters within a single, few-millimetre structure, we eliminate gradient-induced measurement errors inherent in spatially separated hybrid sensors. Furthermore, through-the-coating HO-FBG fabrication maintains the mechanical integrity of the optical fibre, avoiding the fragility of tapered fibres or the weakened fusion points found in spliced fibres. This mechanical resilience is essential for long-term reliability in harsh environments, where spliced or geometrically modified fibres are prone to failure.

Appropriate selection of HO-FBG harmonics, together with precise tailoring of the grating period, enables excellent versatility in matching resonance peak wavelengths to the spectral range of any device (interrogator) available on the market. Finally, a high degree of flexibility in HO-FBG design makes it easy to scale up the dual-parameter single-grating sensing solution towards a high-spectral-adaptability multi-HO-FBG quasi-distributed temperature and strain measurement system. However, when designing measurement systems based on cascaded HO-FBGs, care must be taken to ensure proper separation of peaks originating from individual gratings. While spectral overlap is not possible if sufficient separation is maintained between reflection orders of the same grating, it may occur between resonant peaks from different gratings under varying temperature/strain conditions. To prevent this overlap, it must be ensured at the HO-FBG design stage that the spacing between the peaks of different gratings is sufficiently large to accommodate potential spectral shifts caused by temperature and strain changes. By using (1)–(4), it is possible to design HO-FBGs with the accurately desired absolute Bragg wavelengths and their mutual separation. To achieve this, an appropriate relationship between the grating period and the Bragg orders must be selected so that the Bragg orders fall within the spectral range of the interrogator. Additionally, to enhance distinguishability within the cascaded configuration, HO-FBGs with distinct reflectivities can be used, without affecting measurement capabilities in the wavelength domain.

Another potential application of the proposed spectrally tailored gratings is multi-band optical filtering.

Acknowledgements

Tomasz Osuch and Mariusz Zdanowicz would like to thank the Ministry of Education and Science for the support of this work (grant no. 7383/IA/SN/2023).

References

[1] Yu, C.-W., Lei, S.-C., Chen, W.-S. & Song, S.-R. Downhole fiber optic temperature-pressure innovative measuring system used in sanshing geothermal test site. *Geothermics* **74**, 190–196 (2018). https://doi:10.1016/j.geothermics.2018.03.005

[2] Peng, J. *et al*. Design and experiment of FBG sensors for temperature monitoring on external electrode of lithium-ion batteries. *IEEE Sens. J.* **21,** 4628–4634 (2021). https://doi.org/10.1109/JSEN.2020.3034257

[3] Qiao, X., Shao, Z., Bao, W. & Rong, Q. Fiber Bragg grating sensors for the oil industry. *Sensors* **17**, 429 (2017). https://doi.org/10.3390/s17030429

[4] Rong, Q. & Qiao, X. FBG for oil and gas exploration. *J. Light. Technol.* **37**, 2502–2515 (2019). https://doi.org/10.1109/JLT.2018.2866326

[5] Esbeen, B. V. *et al*. Smart railway traffic monitoring using fiber Bragg grating strain gauges. *Sensors* **22**, 3429 (2022). https://doi.org/10.3390/s22093429

[6] Al-Tarawneh, M., Huang, Y., Lu, P. & Tolliver. D. Vehicle classification system using in-pavement fiber Bragg grating sensors. *IEEE Sens. J.* **18**, 2807–2815 (2018). https://doi.org/10.1109/JSEN.2018.2803618

[7] Song, H., Pei, H. & Zhu, H. Monitoring of tunnel excavation based on the fiber Bragg grating sensing technology. *Measurement* **169**, 108334 (2021). https://doi.org/10.1016/j.measurement.2020.108334

[8] Zheng, R. *et al*. Investigation of measurability and reliability of adhesive-bonded built-in fiber Bragg grating sensors on steel wire for bridge cable force monitoring. *Measurement* **129**, 349–357 (2018). https://doi.org/10.1016/j.measurement.2018.07.053

[9] Zhao, Y., Zhang, N. & Si, G. A fiber Bragg grating-based monitoring system for roof safety control in underground coal mining. *Sensors* **16**, 1759 (2016). https://doi.org/10.3390/s16101759

[10] Presti, D. L. *et al*. Fiber Bragg gratings for medical applications and future challenges: A review. *IEEE Access* **8**, 156863–156888 (2020). https://doi.org/10.1109/ACCESS.2020.3019138

[11] Tosi, D. *et al*. Fiber-optic chirped FBG for distributed thermal monitoring of ex-vivo radiofrequency ablation of liver. *Biomed. Opt. Express* **5**, 1799 (2014). https://doi.org/10.1364/BOE.5.001799

[12] Sypabekova, M. *et al*. Functionalized etched tilted fiber Bragg grating aptasensor for label-free protein detection. *Biosens. Bioelectron.* **146**, 111765 (2019). https://doi.org/10.1016/j.bios.2019.111765

[13] Patrick, H. J., Williams, G. M., Kersey, A. D., Pedrazzani, J. R. & Vengsarkar, A. M. Hybrid fiber Bragg grating/long period fiber grating sensor for strain/temperature discrimination. *IEEE Photon. Technol. Lett.* **8**, 1223–1225 (1996). https://doi.org/10.1109/68.531843

[14] Liu, H. *et al*. Strain measurement at high temperature environment based on Fabry-Perot interferometer cascaded fiber regeneration grating. *Sens. Actuators A: Phys.* **248**, 199–205 (2016). https://doi.org/10.1016/j.sna.2016.07.028

[15] Frazão, O., Melo, M., Marques, P .V. S. & Santos, J. L. Chirped Bragg grating fabricated in fused fibre taper for strain–temperature discrimination. *Meas. Sci. Technol.* **16**, 984–988 (2005). https://doi.org/10.1088/0957-0233/16/4/010

[16] James, S., Dockney, M. & Tatam, R. Simultaneous independent temperature and strain measurement using in-fibre Bragg grating sensors. *Electron. Lett.* **32**, 1133 (1996). https://doi.org/10.1049/el:19960732

[17] Hu, Q. *et al*. Simultaneous measurement of temperature and strain using double-cladding fiber based hybrid Bragg grating. *OSA Contin.* **3**, 1031 (2020). https://doi.org/10.1364/OSAC.389645

[18] Frazão, O. & Santos, J. L. Simultaneous measurement of strain and temperature using a Bragg grating structure written in germanosilicate fibres. *J. Opt. A-Pure Appl. Opt.* **6**, 553–556 (2004). https://doi.org/10.1088/1464-4258/6/6/010

[19] Cavaleiro, P., Araujo, F., Ferreira, L., Santos, J. & Farahi, F. Simultaneous measurement of strain and temperature using Bragg gratings written in germanosilicate and boron-codoped germanosilicate fibers. *IEEE Photon. Technol. Lett.* **11**, 1635–1637 (1999). https://doi.org/10.1109/68.806871

[20] Li, X., Wang, D., Zhao, F. & Dai, E. Simultaneous independent temperature and strain measurement using one fiber Bragg grating based on the etching technique. *Microw. Opt. Technol. Lett.* **43**, 478–481. https://doi.org/10.1002/mop.20507

[21] Chen, G. *et al*. Simultaneous strain and temperature measurements with fiber Bragg grating written in novel hi-bi optical fiber. *IEEE Photon. Technol. Lett.* **16**, 221–223 (2004). https://doi.org/10.1109/LPT.2003.820117

[22] Caucheteur, C., Lhommé, F., Chah, K., Blondel, M. & Megret, P. Novel technique for the simultaneous measurement of strain and temperature using polarization maintaining fiber Bragg gratings, *Proc. SPIE* **5855**, 703–706 (2005). https://doi.org/10.1117/12.623419

[23] Chehura, E., James S. W. & Tatam, R. P. Simultaneous, independent measurement of temperature and strain using a tilted fibre Bragg grating. *Proc. SPIE* **6619**, 66190I (2007). https://doi.org/10.1117/12.738371

[24] Takeda, S., Sato, M. & Ogasawara, T. Simultaneous measurement of strain and temperature using a tilted fiber Bragg grating. *Sens. Actuators A: Phys.* **335**, 113346 (2022). https://doi.org/10.1016/j.sna.2021.113346

[25] Brady, G. *et al*. Simultaneous measurement of strain and temperature using the first- and second-order diffraction wavelengths of Bragg gratings. *IEE Proc.-Optoelectron.* **144,** 156 (1997). https://doi:10.1049/ip-opt:19971373

[26] Xu, M. G., Reekie, L., Dakin, J. P. & Archambault, J. L. Discrimination between strain and temperature effects using dual-wavelength fibre grating sensor. *Electron. Lett.* **30**, 1085–1087 (1994). https://doi:10.1049/el:19940746

[27] Grobmic, D., Mihailov, S. J., Smelser, C. W. & Walker, R. B. Multiparameter sensor based on single high-order fiber Bragg grating made with IR-femtosecond radiation in single-mode fibers. *IEEE Sens. J.* **8**, 1223–1228 (2008). https://doi.org/10.1109/JSEN.2008.926186

[28] Zhu, Y. Mei, H. Zhu, T. Zhang, J. & Yin, S. Dual-wavelength FBG inscribed by femtosecond laser for simultaneous measurement of high temperature and strain. *Chin. Opt. Lett.* **7**, 675–678 (2009). https://doi.org/10.3788/COL20090708.0675

[29] Jin, W., Michie, W. C., Thursby, G., Konstantaki, M. & Culshaw, B. Simultaneous measurement of strain and temperature: error analysis. *Opt. Eng.* **36**, 598–609 (1997). https://doi.org/10.1117/1.601233